International Journal of Thermal Sciences 49 (2010) 635–642

Contents lists available at ScienceDirect

International Journal of Thermal Sciences

journal homepage: www.elsevier.com/locate/ijts

Effect of substrate thickness and material on heat transfer in microchannel heat sinks

Ali Koşar*

Mechatronics Engineering Program, Sabancı University, Tuzla 34956, Istanbul, Turkey

ARTICLE INFO

Article history:
Received 6 March 2009
Received in revised form
4 November 2009
Accepted 4 November 2009
Available online 1 December 2009

Keywords:
Microchannels
Forced convection
Conjugate effects
Micro-heat sinks
Microscale cooling

ABSTRACT

Heat and fluid flow in microchannels of size (200μm × 200 μm, 5 cm long) of different substrate thicknesses (t = 100 μm–1000 μm) and different MEMS (Microelectromechanical Systems) materials (Polyimide, Silica Glass, Quartz, Steel, Silicon, Copper) was studied to observe the effects of thermal conductivity and substrate thickness on convective heat transfer in laminar internal flows.

The results of the model were first validated by the theoretical results recommended by standard forced convection problem with H1 (Constant heat flux boundary condition) condition before the results from the actual microchannel configurations were obtained. Thereafter, general Nusselt number results were obtained from the models of many microchannel configurations based on the commercial package COMSOL MULTIPHYSICS® 3.4 and were discussed on both local and average basis.

A general Nusselt number correlation for fully developed laminar flow was developed as a function of two dimensionless parameters, namely Bi, Biot number and relative conductivity k^*, to take the conduction effects of the solid substrate on heat transfer into account. It was also demonstrated when the commonly used assumption of constant heat flux boundary (H1) condition is applicable in heat and fluid flow analysis in microfluidic systems. For this, a new dimensionless parameter was employed. A value of 1.651 for this suggested dimensionless parameter ($Bi^{0.04}k^{*-0.24}$) corresponds to 95% of the Nusselt number associated with the constant heat flux boundary condition so that it could be set as a boundary for the applicability of constant heat flux boundary (H1) condition in microfluidic systems involving heat transfer.

© 2009 Elsevier Masson SAS. All rights reserved.

1. Introduction

Heat and fluid flow in micro domains has been attracting great attention in the heat transfer community during the last decade. The enhancement in convective heat transfer with diminishing size has been exploited in many applications such as in microengines [1–3], microreactors [4–6], thermal microactuators [7], and drug delivery systems [8,9]. As a result, extensive literature reviews on heat and fluid flow in microscale have been emerging during the past decade to summarize copious research efforts in this field [10–13].

In most of the cases, convective heat transfer in microfluidic systems is coupled with significant conduction effects existing within substrates. This coupling is becoming more significant as the material selection is shifting from Silicon-based devices to polymer and glass substrates thanks to the cheap soft lithography based microfabrication capabilities. Regardless the substrate material and thickness, however, most of heat transfer analyses are performed under the assumption of constant heat flux boundary (H1) condition. There may be cases though where conjugate effects play an important role in imposing different boundary conditions for convective heat transfer, so that commonly used constant heat flux boundary (H1) condition assumption may not be valid in such configurations anymore. This could be particularly the case where thick and low thermal conductivity (such as polymers like PDMS, PMMA) substrates are utilized. Hence, to better describe the convective heat transfer in micro domains, conjugate effects should be considered.

Numerical studies have been performed for micro-heat sinks with single-phase flow by many researchers to investigate their thermal performances and the conjugate effects [14–21]. Fedorov and Viskanta [14] studied three dimensional conjugate heat transfer in a microchannel heat sink and unveiled the potential of microchannel heat sinks for the electronics cooling applications. They also obtained large temperature gradients, which might cause thermal and structural failure of the heat sink. Li et al. [15] emphasized that thermophysical properties of the liquid significantly affect heat and fluid flow in 10 mm long Silicon microchannels (57 wide and 180 deep) and found out that for Reynolds number lower than 200 and

* Tel.: +90 216 483 9621; fax: +90 216 483 9550.
E-mail address: kosara@sabanciuniv.edu

1290-0729/$ – see front matter © 2009 Elsevier Masson SAS. All rights reserved.
doi:10.1016/j.ijthermalsci.2009.11.004

Nomenclature

A_c	cross sectional area (m^2)
A_s	surface area (m^2)
Bi	Biot number
c_p	specific heat at constant pressure (kJ kg^{-1} °C^{-1})
d_h	hydraulic diameter (m)
f	friction factor
G	mass velocity (kg m^{-2} s^{-1})
h	local heat transfer coefficient (W m^{-2} K^{-1})
$\overline{h}$	average heat transfer coefficient (W m^{-2} K^{-1})
H	channel height (m)
k^*	dimensionless thermal conductivity (W m^{-1} °C^{-1})
k_{fluid}	thermal conductivity of the fluid (W m^{-1} °C^{-1})
k_s	thermal conductivity of the surface (W m^{-1} °C^{-1})
L	channel length (m)
Nu_z	local Nusselt number
$\overline{Nu}$	average Nusselt number
$\vec{n}$	normal vector
q''_{app}	applied heat flux (W m^{-2})
p	pressure (Pa)
Pr	Prandtl number
Re	Reynolds number
t	substrate thickness (m)
T	temperature (°C)
$\overline{T}_{f,av}$	average fluid temperature along the entire microchannel (°C)
$\overline{T}_{f,z}$	average fluid temperature along the entire cross section at a certain longitudinal location z (°C)
$\overline{T}_{s,av}$	average surface temperature along the entire microchannel (°C)
$\overline{T}_{s,z}$	average surface temperature along the entire cross section at a certain longitudinal location z (°C)
u	velocity in longitudinal direction (m s^{-1})
V	microchannel volume (m^3)
$\vec{V}$	velocity vector (m s^{-1})
W	channel width (m)
W_2	width in Fig. 2 (m)
x	location in x axis
y	location in y axis
z	location in z axis

Greek

Δp	pressure drop (kPa)
μ	viscosity (kg m^{-1} s^{-1})
ρ	density (kg m^{-3})

Subscript

av	average
HF	constant heat flux boundary (H1)
f	fluid
s	surface
sub	substrate
w	wall

$d_h/L < 0.01$ fully developed laminar flow assumption is valid. Barba et al. [16] studied heat transfer in a polymeric heat sink and presented it as a futuristic heat sink with low cost. Morini [17] focused on scaling effects for liquid flows in microchannels. The author proposed limits for viscous dissipation, and conjugate effects as a function of Nusselt number and stated that the conduction inside the channel wall would have a tendency to reduce the mean Nusselt number under certain circumstances, and for high Reynolds numbers, the entrance and viscous dissipation effects became more dominant. Li and Peterson [18] investigated 3D conjugate heat transfer in Silicon-based microchannels. The authors optimized the geometry to reach to a minimum value of thermal resistance and obtained a significantly better performance at the same pumping power compared to the old studies (Tuckerman and Pease [22]). Wei et al. [19] investigated heat and fluid flow in a stacked silicon microchannel heat sink and achieved outstanding cooling performances. They observed significant effects of coolant flow direction on heat transfer performance and obtained a better temperature uniformity with the parallel flow arrangement compared to the counterflow arrangement. In the conjugate heat transfer study of Lelea [20] on partially heated microtubes made of copper, silicon and stainless steel, local Nusselt number distribution complied with the theory for the non-axial conduction case, which was observed at intermediate and high Reynolds numbers ($Re > 200$). The author also emphasized on the effect of the wall thickness and material on the heat transfer. Mlcak et al. [21] studied laminar flow and heat transfer in a parallel array of rectangular microchannels with a hydraulic diameter of 86.6 μm and found that for the same hydraulic diameter, thermal resistance and friction coefficient values changed insignificantly for aspect ratios larger than 0.5, whereas values of thermal resistances decreased with aspect ratio at lower aspect ratios.

The current study addresses to the aforementioned need for the information about the conjugate effects on heat transfer in microchannels. In this study, it was aimed at clearly displaying the cases in which the constant heat flux boundary condition (H1) is applicable so that the use of this common assumption in heat and fluid flow could be verified. For this purpose, heat and fluid flow in microchannels of standard size (200μm × 200 μm) with different wall thicknesses ($t = 100$ μm, $t = 1000$ μm) made of standard MEMS (Microelectromechanical Systems) materials (Polyimide, Silica Glass, Quartz, Steel, Silicon, Copper) was modeled using the commercial package COMSOL MULTIPHYSICS® 3.4. General Nusselt number trends were discussed for both local and average Nusselt numbers, which were obtained from the models of many microchannel configurations. The effects of microchannel material and substrate thickness on heat transfer were revealed. Finally, a general Nusselt number correlation for fully developed laminar flow applicable to any material and substrate thickness was presented as a function of two dimensionless parameters: Bi, Biot number and k^* relative conductivity.

2. Model

The microchannel configurations used in the current study were modeled by commercial multiphysics software COMSOL MULTIPHYSICS® 3.4, which can solve Continuity, Navier Stokes and Energy equations for both the solid and fluid subdomains simultaneously. As a result, temperature, pressure, and velocity distributions across a microchannel heat sink were found under a broad range of Reynolds number and heat flux using water as working fluid.

A general model for the microchannel configuration is displayed in Fig. 1. As seen in this figure, the working fluid flows through the microchannel, which is surrounded by the solid substrate and a glass cover. Such an arrangement is typically used in microfluidic devices such as drug delivery, microreactor and micro mixers, which are heated from their bottom surface and have a transparent cover for visualization purposes. Accordingly, the microchannel is heated from the bottom of the solid substrate with a fixed heat flux

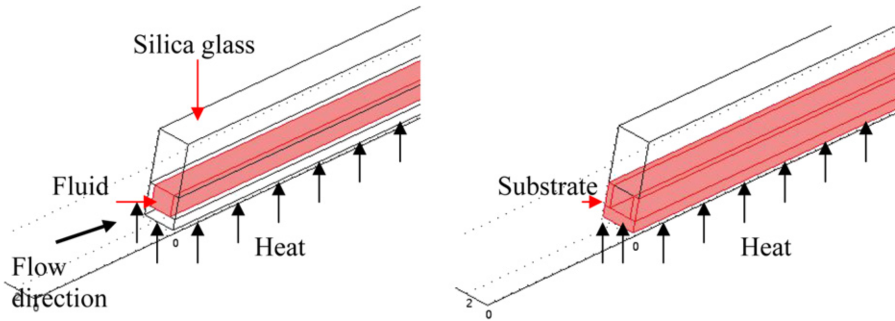

Fig. 1. a) Water subdomain b) Heat transferring solid subdomain.

(Fig. 1), and heat and fluid flow are analyzed under steady state conditions. For steady laminar flow, the Navier-Stokes equations for incompressible fluids are used as the governing equations of the flow along with the continuity equation:

$$\vec{V}\cdot\nabla(\rho\vec{V}) = -\nabla P + \nabla\cdot(\mu\nabla\vec{V}) \tag{1}$$

$$\nabla\cdot\vec{V} = 0 \tag{2}$$

In the above equations, working fluid density (ρ) and viscosity (μ) are considered as a function of temperature (T) to account for the change in the fluid property due to heating.

As an input parameter, fluid velocity at the inlet is set to be a non-zero value to drive the fluid in the channel as:

$$\vec{V}\cdot\vec{n}|_{x=0,y,z} = u_{in} = \frac{G}{\rho_F} \tag{3}$$

At the outlet of the channel, the outlet pressure is kept as the zero value (gauge pressure):

$$-P\vec{i}\cdot\vec{n}|_{x=L,y,z} = 0 \tag{4}$$

Inside the substrate and glass cover and along the channel walls non-slip boundary condition is applied. This condition is based on the continuum assumption provided by small Knudsen numbers ($Kn < 0.01$), which is mostly the case of fluid flow in microscale.

Reynolds number (Re) is evaluated by using the mass velocity, hydraulic diameter, and viscosity as:

$$\mathrm{Re} = \frac{Gd_h}{\mu} \tag{5}$$

Friction factor (f) is defined as a function of pressure drop across the channel (ΔP) and mass velocity (G):

$$f = \frac{2\Delta P\rho_F d_h}{G^2 L} \tag{6}$$

As a complementary module, heat transfer equation is solved simultaneously with the flow problem for the fluid subdomain. A steady and incompressible laminar flow is assumed in the model. Moreover, thermal radiation (due to relatively low temperatures) and viscous dissipation (due to low Brinkman numbers) are also neglected, and continuum assumption was made. As a result of these assumptions, heat transfer is governed by the following equation:

$$\rho c_p\vec{V}\cdot\nabla T = \nabla k\nabla T \tag{7}$$

The fluid temperature at the inlet is equated to T_{in} while convective flux boundary condition is utilized at the exit of the channel. Steady state heat conduction equation is valid inside both substrate and transparent glass cover subdomains:

$$\nabla k_w\nabla T_w = 0 \tag{8}$$

A uniform heat flux is imposed from below into the substrate, while the other outer boundaries for both the substrate and glass cover are thermally isolated. In addition, the temperature and heat flux of the fluid at its substrate and glass boundary are equated to the temperature and heat flux of the solid (conjugate boundary conditions) due to continuity between solid and fluid phases.

When the temperature profile is obtained, temperature profile is processed to find local and average Nusselt numbers. At a certain axial location z, the local Nusselt number is found from the following expressions as a function of the heat flux applied from the bottom (Fig. 2):

$$Nu_z = \frac{hd_h}{k_F} \tag{9}$$

where

$$h = \frac{q''_{app}W_2}{2(W+H)\left(\overline{T}_{s,z} - \overline{T}_{f,z}\right)} \tag{10}$$

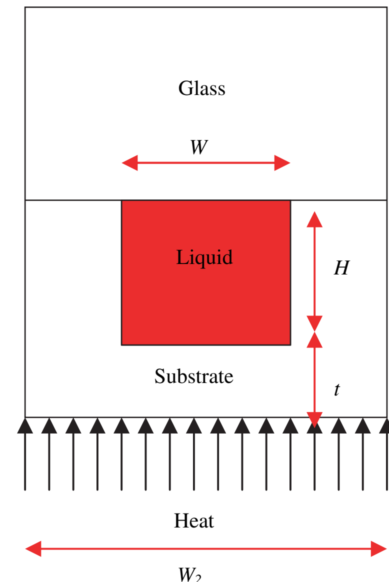

Fig. 2. Overview of the cross sectional area of the microchannel configuration at any z location.

$$\overline{T}_{f,z} = \frac{1}{A_c}\iint\limits_{A_c} T_{f,z}(x,y)dA_c \quad (11)$$

$$\overline{T}_{s,z} = \frac{1}{2(W+H)}\oint\limits_{\text{wall}} T_{s,z}(x,y)dS_{\text{sub+glass}} \quad (12)$$

The above expression is used for different microchannel configurations with different substrate materials and substrate thicknesses so that the effect of substrate material and substrate thickness on local Nusselt numbers could be revealed. At the same time, it will be examined whether the theoretical Nusselt numbers corresponding to constant heat flux boundary condition (H1) are obtained.

The same approach will be followed for average Nusselt numbers. For this case, the following expressions are used in the light of the analysis for local Nusselt numbers:

$$\overline{Nu} = \frac{\overline{h}d_h}{k_F} \quad (13)$$

where

$$\overline{h} = \frac{q''_{app}W_2}{2(W+H)\left(\overline{T}_{s,av} - \overline{T}_{f,av}\right)} \quad (14)$$

$$\overline{T}_{f,av} = \frac{1}{V}\int\int\limits_{V}\int T_f(x,y,z)dV \quad (15)$$

$$\overline{T}_{s,av} = \frac{1}{2(W+H)L}\iint\limits_{\text{wall}} T_s(x,y,z)dA_{\text{sub+glass}} \quad (16)$$

In this multiphysics problem, fluid and solid domains have different mesh configurations to reduce the mesh elements and increase the performance at the same time. A typical configuration consists of approximately 252 485 degrees of freedom and 37 754 tetrahedral mesh elements. A typical temperature distribution for the entire geometry (Fig. 3a) and a typical temperature distribution of a point at the microchannel cross section surface along the longitudinal direction (Fig. 3b) are demonstrated in Fig. 3 as a sample. These

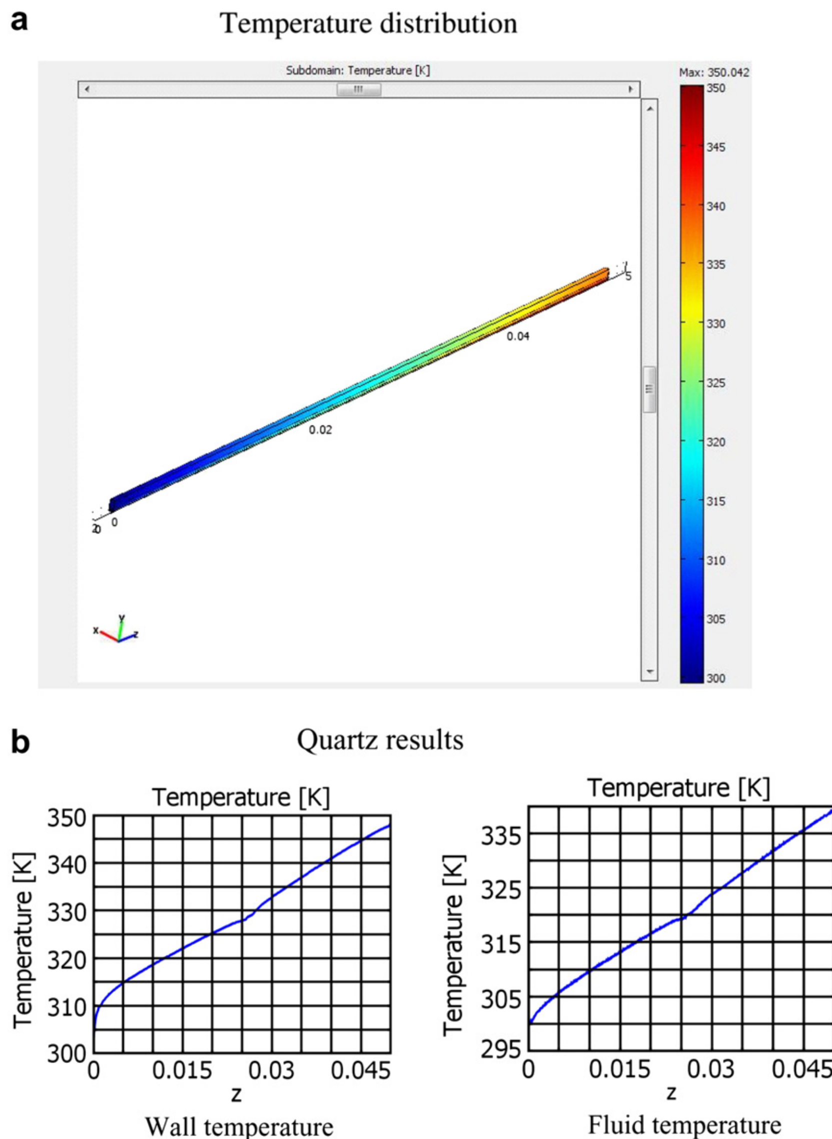

Fig. 3. Mesh overview of the channel and typical temperature distribution. (a) Temperature distribution, (b) Quartz results.

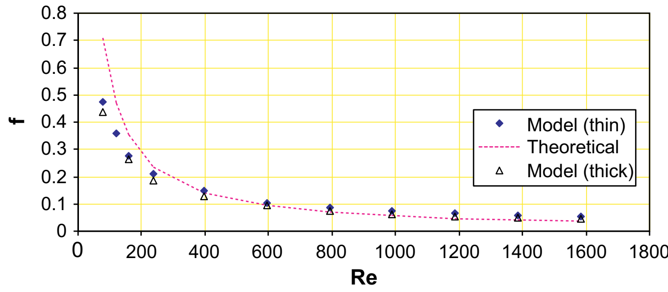

Fig. 4. Friction factor profile for constant heat flux boundary condition.

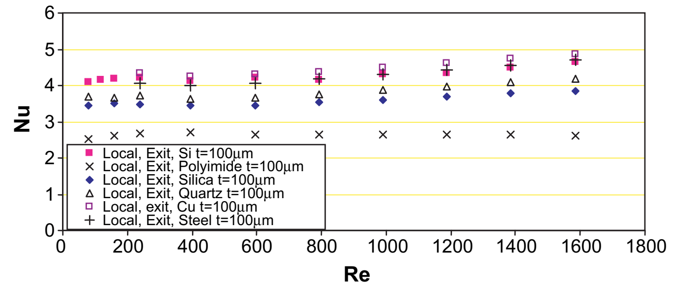

Fig. 6. Local Nusselt numbers for different substrate materials (t = 100 μm).

numbers were selected to make sure of the independence of the solution on the mesh element number. Indeed, approximately 100 000 tetrahedral mesh elements resulted in a local Nusselt number value (Nu = 4.81, Re = 1188, q'' = 250 000 W/m^2, Copper thin substrate, t = 100 μm) with a difference less than 3% compared to a typical mesh (Nu = 4.73) in the current study suggesting the achievement of mesh element number independence.

3. Results and discussion

This section displays hydrodynamic and heat transfer results of the current study. First, the validation of the model is included. Thereafter, the effects of substrate material and substrate thickness on heat transfer are discussed. Finally, a new prediction tool for Nusselt number is introduced, and its broad applicability potential is emphasized.

3.1. Validation of the model

Fig. 4 demonstrates a representative friction factor profile (silicon substrate for both thin (t = 100 μm) and thick (t = 1000 μm) wall configurations) over Reynolds numbers under laminar flow conditions (Re < 2000, q'' = 50,000–250,000 W/m^2). It could be observed that the results of the model are in good agreement with the theoretical prediction ($f = C$/Re, C = 56.02) recommended for laminar flows under adiabatic conditions. The model results at low Reynolds numbers (Re < 400) are below the theoretical predictions. The reason for this is the heating provided from the bottom. Due to the heating, the viscosity of the liquid drops, which leads to a drop in the pressure and thus in friction factor. The temperature rise is more significant at low flow rates and Reynolds numbers. As a result, the deviation of the model from the theory becomes more at low Reynolds numbers. The results between thin wall (t = 100 μm) and thick wall configurations (t = 1000 μm) are due to different temperature distribution provided by conjugate effects.

Fig. 5 displays the comparison between the theoretical prediction of Nusselt number for laminar developed flow (Nu = 3.6 in rectangular channels with aspect ratio of one for laminar developed flow at constant heat flux boundary condition) and the model results obtained from a 200 × 200 μm microchannel at constant heat flux boundary condition (imposed on all of the microchannel walls for this specific case). As can be seen from the figure, there is a very good agreement between the model results and the theoretical prediction for Re < 976. Beyond Re = 1000 Nusselt number results are greater than the theoretical value of Nusselt number for developed flows. This can be explained by the fact that the thermal entry length at this critical Reynolds number (about 1000) is the same as the microchannel length (L = 0.05 m = 0.056Re × d_h × Pr, where Pr ~ 4.7). Indeed, the value at Re = 1672 is higher than the theoretical Nusselt number value at constant heat flux boundary conditions for developed laminar flows.

3.2. Effect of thermal conductivity

Figs. 6 and 7 display the effect of thermal conductivity on heat transfer for microchannels of the same size and substrate thickness. For microchannel materials of high conductivity, both average and local (evaluated at the exit) Nusselt numbers converge to a certain value at low Reynolds numbers (Re < 400). The average Nusselt number is affected by developing flow effects more than the local Nusselt number at the exit since a portion of the microchannel has already a developing flow region due to entrance effects. As Reynolds number is increased, entrance effects augment, and average Nusselt number profile starts to deviate from the local Nusselt number profile. At a certain Reynolds number (Re ~ 1000), local Nusselt number at the exit also starts to increase due to the arrival of developing effects to the exit.

For low conductivity microchannel materials (Polyimide), the profiles become different. The Nusselt number is lower for this case (more than one) than the Nusselt number obtained from the Silicon case. This decrease could be attributed to the increased conduction resistance along the microchannel wall due to much lower thermal conductivity in Polyimide microchannels (more than 1000 times than in Silicon microchannels). This proves the conduction effects on the heat transfer in micro domains and implies that constant heat flux is not always valid. Such a decrease was also reported in the previous studies [17,23]. It can be inferred that for high thermal conductivity

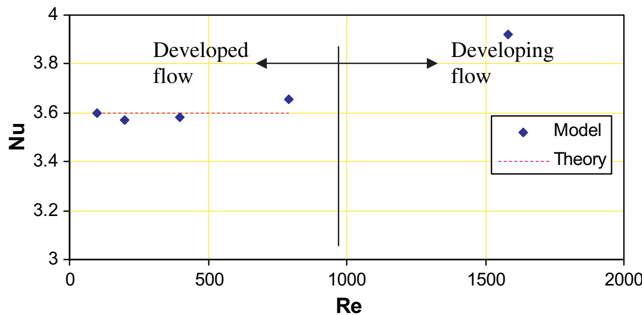

Fig. 5. Nusselt number profile for constant heat flux boundary condition.

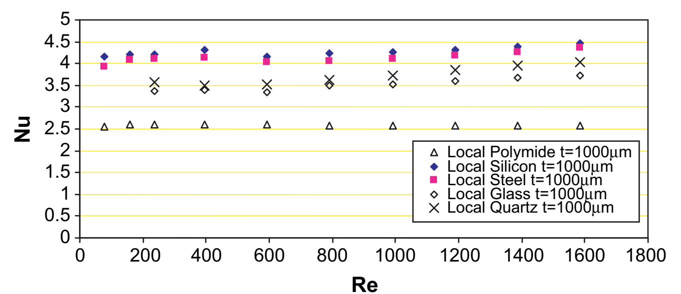

Fig. 7. Local Nusselt numbers for different substrate materials (t = 1000 μm).

materials, constant heat flux boundary condition can be used, however, for low thermal conductivity materials a significant deviation from the constant heat flux boundary condition occurs. The nonlinear axial surface temperature distribution at given y and z positions (the corner point on the lower edge of the cross section was chosen) at the channel wall cross section supports this conclusion (Fig. 8) while for Quartz the temperature profile is significantly more linear.

Fig. 6 demonstrates the local exit Nusselt numbers along with Reynolds numbers for Polyimide, Glass Silica, Quartz, Steel, Silicon, and Copper materials in thin wall microchannels. It can be seen that the lowest Nusselt numbers are present in Polyimide made microchannels, which have the lowest thermal conductivity. The profile is constant over the entire Reynolds number range for this configuration. As thermal conductivity is increased, the Nusselt number shifts to a higher value. Nusselt numbers for Silica Glass microchannels are higher (more than 0.5) than for Polyimide. However, after a certain thermal conductivity value (starting from Steel), the Nusselt numbers converge to a certain limit. Due to the different heating configuration, the Nusselt number value at the convergence is not the same as that for uniformly heated rectangular microchannels with constant heat flux boundary condition ($Nu = 3.6$ for developed flow at constant heat flux boundary condition). However, it can be still regarded as the Nusselt number value associated with constant heat flux boundary condition in the current configuration.

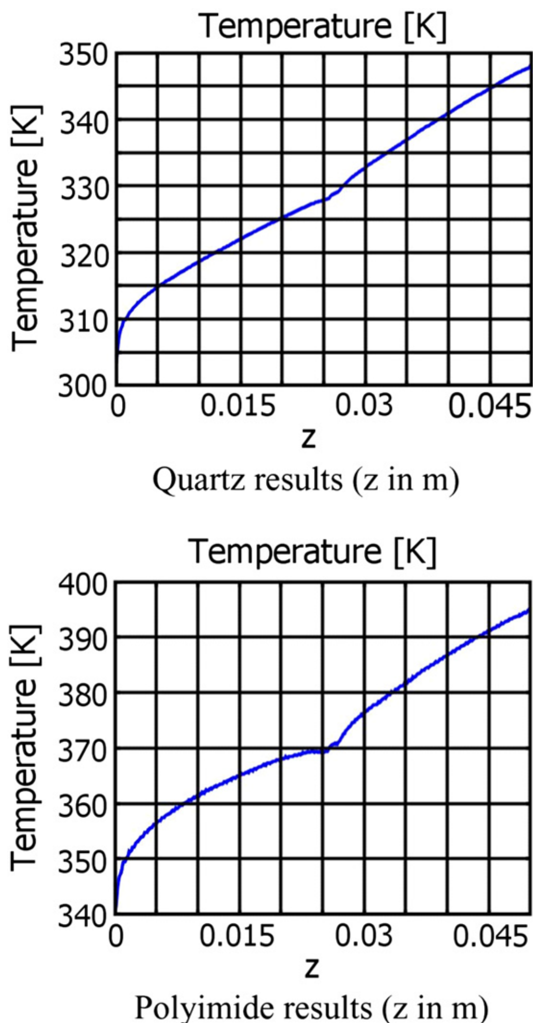

Fig. 8. Axial Temperature variations in Quartz and Polyimide at the corner point on the lower edge of the cross section. Quartz results (z in m), Polyimide results (z in m).

3.3. Effect of substrate thickness

The thick wall results are similar to thin wall results in terms of the magnitude of Nusselt numbers for Si, Steel, and Copper microchannels (Figs. 6, 7 and 9). This suggests that constant heat flux boundary condition is prevalent for these materials in both thin and thick substrate configurations. Nusselt number does also not change with the substrate thickness for Polyimide and Silica Glass having a low thermal conductivity (Fig. 9a,b).

For intermediate thermal conductivities, local Nusselt numbers change with the substrate thickness as can be seen from Fig. 9c. This is reflected in the Nusselt number values, which are between Polyimide and Copper microchannel cases. In this case, Nusselt number changes moderately with substrate thickness different from other materials. In the thick substrate configuration, Nusselt numbers are lower than in the thin substrate configuration. Similar trends are present for average Nusselt numbers.

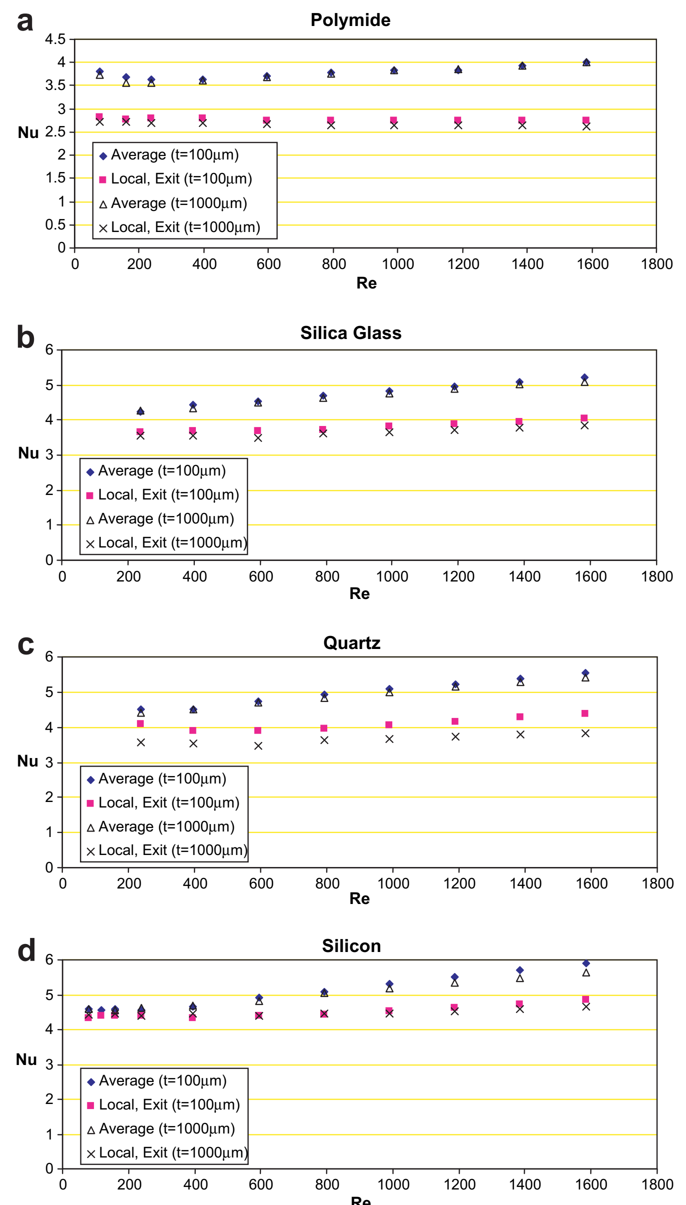

Fig. 9. Local and Average Nusselt numbers for different substrate materials. a) Polyimide, b) Silica Glass, c) Quartz, d) Silicon.

The weaker dependence of substrate thickness on Nusselt number compared to the effect of thermal conductivity is because there exists a constraint in the ratio of substrate thickness to the microchannel size. It is very unlikely to use substrate thicknesses much thicker than the microchannel size, whereas the thermal conductivity could be varied by larger quantities. Thus, the change in the thermal resistance due to conduction is mostly produced by the change in the thermal conductivity, and Nusselt number is consequently more likely to be changed by varying the thermal conductivity.

3.4. New Nusselt number correlation

A Nusselt number correlation taking the conjugate effects into account is sought to predict the convective heat transfer in microchannels of different materials and substrate thicknesses for fully developed flows. Biot number ($=h_{HF}t/k_{solid}$), which is a function of the substrate thickness (t) and represents the ratio of conduction in the solid to the convection, and the dimensionless conductivity k^* ($=k_{solid}/k_{Copper}$) are employed as dimensionless numbers to develop a general correlation. This approach is based on the conjugate heat transfer analysis performed in the literature [17,20,23].

Biot number mainly includes the substrate thickness effect, whereas the dimensionless conductivity determines the relative magnitude of thermal conductivity to that of Copper (extreme case) and covers the thermal conductivity effects.

In an attempt to predict the Nusselt number for developed flow conditions, the following correlation was developed:

$$Nu = 4.516 - 0.2551\frac{Bi^{0.04}}{k^{*0.24}} \tag{17}$$

The above correlation can provide excellent prediction to the model results with a MAE of 1.02%. In addition, it can also follow the trends in Nusselt number profiles for all materials examined in the current study. As can be seen from Fig. 10, all the model results could be represented by the above correlation within $\pm5\%$. The above correlation can be transformed into a nondimensional format (an expression of the ratio of the Nusselt number with conjugate effects to Nusselt number for constant heat flux boundary condition) as:

$$\frac{Nu}{Nu_{HF}} = 1.048 - 0.0592\frac{Bi^{0.04}}{k^{*0.24}} \tag{18}$$

Using the above equation, Nusselt number can be estimated for any configuration with any material and any substrate thickness. Hence, this correlation has the potential use of having great applicability in many fields like drug delivery, microreactors, fuel cells, and micro-heat sinks, which have dimensions providing the validity of continuum assumption. Moreover, it could act as a boundary for the constant heat flux boundary condition in microsystems. A value of 1.651 for the dimensionless parameter $Bi^{0.04}k^{*-0.24}$ (included in the developed correlation) corresponds to 95% of the Nusselt number associated with the constant heat flux boundary condition. Thus, this value could be a lower boundary for the applicability of this heat flux boundary condition in the heat and fluid flow in microfluidic systems.

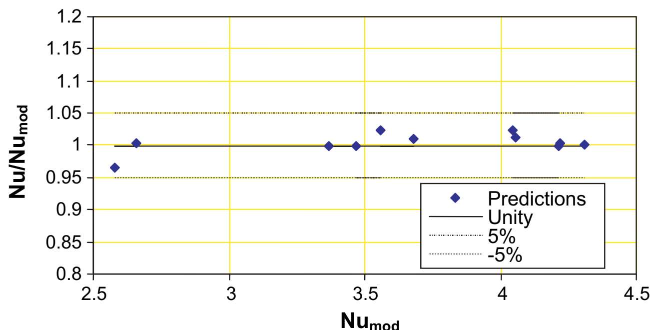

Fig. 10. Prediction capability of the new correlation.

4. Conclusions

Heat and fluid flow in microchannels was investigated to observe the substrate thickness and material thermal conductivity effects on convective heat transfer in laminar internal flows. After the validation of the model developed in MULTIPHYSICS® 3.4 with the theory, the effect of thermal conductivity and substrate thickness on convective heat transfer was discussed in detail for the conjugate heat transfer conditions involving the interaction between conduction in the solid subdomains (transparent glass cover, substrate) and forced convection in the liquid subdomain. Below are important findings of the current study:

- In a validation effort of the model, a very good agreement between the model results and the theoretical prediction corresponding to constant heat flux boundary condition for $Re < 976$ was observed. Beyond $Re = 1000$ Nusselt number results were greater than the theoretical value of Nusselt number for developed flows due to developing effects.
- For microchannel materials of high conductivity, both average and local (at the exit) Nusselt numbers converge to a certain value at low Reynolds numbers ($Re < 400$). The average Nusselt number is affected by developing flow effects more than the local Nusselt number at the exit since a portion of the microchannel has already a developing flow region.
- The Nusselt number is lower for low thermal conductivity materials than the Nusselt number obtained from high conductivity materials. This finding suggests that for low thermal conductivity materials, a significant deviation from the constant heat flux boundary condition occurs.
- The change in the thermal resistance due to conduction is mostly produced by the change in the thermal conductivity rather than the substrate thickness. The weaker dependence of substrate thickness on Nusselt number compared to the effect of thermal conductivity is because of the existing constraint in the ratio of substrate thickness to the microchannel size.
- A new correlation was developed to predict Nusselt number in microchannel heat sinks of any material and any substrate thickness. It has the potential use of having great applicability in many fields like drug delivery, microreactors, fuel cells, and micro-heat sinks and could propose a lower boundary for the constant heat flux boundary (H1) condition assumption in microsystems.

Acknowledgements

The author is thankful to Mr. Ahmet Fatih Tabak from Sabancı University, Istanbul for his valuable comments. This work was supported TUBITAK (The Scientific and Technological Research Council of Turkey) Support Program for Scientific and Technological Research Projects Grant, 107M514.

References

[1] X. Yang, A. Holke, S.A. Jacobson, J.H. Lang, M.A. Schmidt, S.D. Umans, An electrostatic, on/off microvalve designed for gas fuel delivery for the MIT microengine. Journal of Microelectromechanical Systems 13 (4) (2004) 660–668.

[2] J.H. Cho, L.W. Weiss, C.D. Richards, D.F. Bahr, R.F. Richards, Power production by a dynamic micro heat engine with an integrated thermal switch. Journal of Micromechanics and Microengineering 17 (9) (2007) 217–223.
[3] Y. Peles, V.T. Srikar, T.S. Harrison, C. Protz, A. Mracek, S.M. Spearing, Fluidic packaging of microengine and microrocket devices for high-pressure and high-temperature operation. Journal of Microelectromechanical Systems 13 (1) (2004) 31–40.
[4] A.L. Dessimoz, L. Cavin, A. Renken, L. Kiwi-Minsker, Liquid–liquid two-phase flow patterns and mass transfer characteristics in rectangular glass micro-reactors. Chemical Engineering Science 63 (16) (2008) 4035–4044.
[5] D. Schafer, J.A. Squier, J. van Maarseveen, D. Bonn, M. Bonn, M. Muller, In situ quantitative measurement of concentration profiles in a microreactor with submicron resolution using multiplex CARS microscopy. Journal of American Chemical Society 130 (35) (2008) 11592–11593.
[6] K. Geyer, H. Wippo, P.H. Seeberger, Microreactors as tools in the synthesis laboratory. Chimica Oggi-Chemistry Today 26 (1) (2008) 23–25.
[7] P. Yang, M. Stevenson, Y.J. Lai, C. Mechefske, M. Kujath, T. Hubbard, Design, modeling and testing of a unidirectional MEMS ring thermal actuator. Sensors and Actuators A-Physical 143 (2) (2008) 352–359.
[8] J.M. Gilliesa, C. Prenanta, G.N. Chimona, G.J. Smethursta, B.A. Dekkera, J. Zweita, Microfluidic technology for PET radiochemistry. Applied Radiation and Isotopes 64 (2006) 333–336.
[9] C.-C. Lee, Sui G. Guodong, A. Elizarov, C.J. Shu, Y.S. Shin, A.N. Dooley, J. Huang, A. Daridon, P. Wyatt, D. Stout, H.C. Kolb, O.N. Witte, N. Satyamurthy, J.R. Heath, M.E. Phelps, S.R. Quake, H.-R. Tseng, Multistep synthesis of a radiolabeled imaging probe using integrated microfluidics. Science 310 (2008) 1793–1796.
[10] S.G. Kandlikar, Two-phase flow patterns, pressure drop, and heat transfer during boiling in minichannels flow passages of compact evaporators. Heat Transfer Engineering 23 (1) (2002) 5–23.
[11] S.G. Kandlikar, Heat transfer mechanisms during flow boiling in micro-channels. Journal of Heat Transfer 126 (1) (2004) 8–16.
[12] J.R. Thome, Boiling in microchannels: a review of experiment and theory. International Journal of Heat and Fluid Flow 25 (2004) 128–139.
[13] B. Agostini, M. Fabbri, J.E. Park, L. Wojtan, J.-R. Thome, B. Michel, State of the art of high heat flux cooling technologies. Heat Transfer Engineering 28 (4) (2007) 258–281.
[14] A.G. Fedorov, R. Viskanta, Three dimensional conjugate heat transfer in the microchannel heat sink for electronic packaging. International Journal of Heat and Mass Transfer 43 (2000) 399–415.
[15] J. Li, G.P. Peterson, P. Cheng, Three dimensional analysis in the micro heat sink with single-phase flow. International Journal of Heat and Mass Transfer 47 (2004) 4215–4231.
[16] A. Barba, B. Musi, M. Spiga, Performance of a polymeric heat sink with circular microchannels. Applied Thermal Engineering 26 (2006) 787–794.
[17] G.L. Morini, Scaling effects for liquid flows in microchannels. Heat Transfer Engineering 27 (2006) 64–73.
[18] J. Li, G.P. Peterson, 3-dimensional numerical optimization of silicon-based high performance parallel microchannel heat sink with liquid flow. International Journal of Heat and Mass Transfer 50 (2007) 2895–2904.
[19] X. Wei, Y. Joshi, M.K. Patterson, Experimental and numerical study of a stacked microchannel heat sink for liquid cooling of microelectronic devices. Journal of Heat Transfer 129 (2007) 1432–1443.
[20] D. Lelea, The conjugate heat transfer of the partially heated microchannels. Heat and Mass Transfer 44 (2007) 33–41.
[21] J.D. Mlcak, N.K. Anand, M.J. Rightley, Three dimensional laminar flow and heat transfer in a parallel array of microchannels etched on a substrate. International Journal of Heat and Mass Transfer 51 (2008) 5182–5191.
[22] D.B. Tuckerman, R.F.W. Pease, High-Performance heatsinking for VLSI. IEEE Electronic Device Letters EDL-2 (1981) 126–129.
[23] G. Maranzana, I. Perry, D. Maillet, Mini- and micro-channels: influence of axial conduction in the walls. International Journal of Heat and Mass Transfer 47 (2004) 3993–4004.